Journal of Materials Chemistry C

Accepted Manuscript

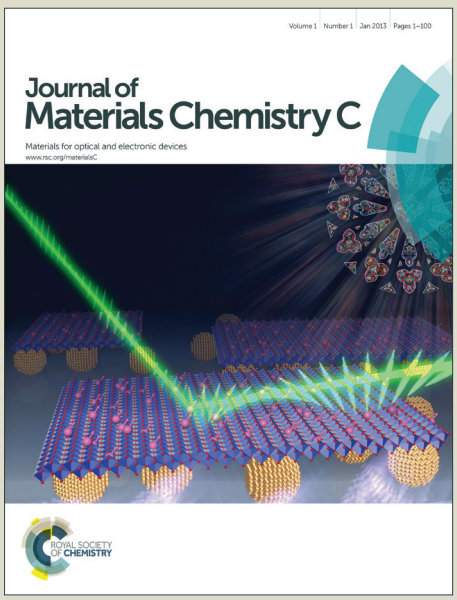

ROYAL SOCIETY OF CHEMISTRY

www.rsc.org/materialsC

Journal of Materials Chemistry C RSCPublishing

ARTICLE

Assembling of a high-scattering photoelectrode using a hybrid nano-TiO_2 paste

Cite this: DOI: 10.1039/x0xx00000x

Jia Lin,[a] Li Zheng,[a] Xiaolin Liu,[b] Shu Zhu,[b] Yongsheng Liu[a] and Xianfeng Chen[*b]

Received 00th January 2012,
Accepted 00th January 2012

DOI: 10.1039/x0xx00000x

www.rsc.org/

The nanostructured architecture of the photoanodes is a key factor limiting the performance of dye-sensitized solar cells (DSSCs). In this study, TiO_2 nanotube (NT) powders were fabricated by anodic growth of NT arrays on titanium foils and ultrasonic dispersion of the obtained NTs. The NTs were collected, annealed and then coated on transparent conductive substrates to form the pure NT photoanodes. The crystallinity of the NTs was optimized at a high annealing temperature. Furthermore, the highly crystallized NT powders were incorporated into TiO_2 nanoparticle (NP) pastes to form NT-NP hybrid pastes and thus hybrid photoanodes were obtained. The embedded NTs served as a light scattering component to trap the incident light inside the dye-sensitized TiO_2 films, leading to the significant enhancement of light absorption. By adjusting the weight ratio of NT/NP, the scattering effect can be optimized. The hybrid photoanode with the optimized film composition (50 wt% NT) provided the highest solar cell efficiency of 6.00% due to the simultaneous improvement of the light scattering, dye anchoring and NT crystallinity. This fabrication strategy is simple, efficient, economical and suitable for large-scale production.

Introduction

In typical dye-sensitized solar cells (DSSC), nanostructured photoanode is a very important component.[1, 2] The functionality of the photoanode can be characterized primarily by three factors: the light harvesting, the electron injection from the dyes to the semiconductor, and the electron collection. The typical photoanode in a DSSC consists of a mesoporous TiO_2 metal oxide nanoparticle (NP) film, which provides a large accessible surface area for loading of dye molecules, and also a unique band structure for the efficient interfacial electron transfer. However, due to the limited electron diffusion lengths and the small light-absorption coefficients of dyes, the photon energy of the solar irradiation has not been fully utilized. A significant portion of the incident light would penetrate the NP film, especially in the long-wavelength region.[3] Consequently, the improvement of light harvesting capacity of the photoanode is critical to the optimization of the solar energy conversion efficiency.

The nano-architecture of the photoelectrodes in DSSCs greatly influences the photon to electron performances. Many efforts have been devoted to tuning the morphologies of TiO_2 films or searching for alternative nanostructures which are beneficial to the improvement of light absorption, charge collection and thus device performance. One representative strategy is the employment of NP photoanodes containing light scattering centers with a high diffuse reflectivity, such as large TiO_2 NPs (200–400 nm),[4, 5] submicrometer-sized solid or hollow spheres,[6, 7] core/shell structures,[8] one-dimensional (1D) rods/fibers/tubes,[9–13] and nano-patterning.[14, 15] Due to the wide-band scattering effect,[16] the incident light can be confined inside the solar cells, leading to the enhanced light harvesting efficiency in a broad spectral range. For various light scattering structures, the improvement of dye adsorption, redox penetration, and electron lifetime is essential to the high performance DSSCs.[7]

The vertically aligned 1D anodic TiO_2 nanotube (NT) architectures have been developed recently for application in DSSCs, which possess many advantages such as the easy fabrication procedures, the slow electron-hole recombination and the enhanced carrier collection.[17–19] In addition, typical NTs have inherent light scattering ability due to the large outer diameters in the range of 100–200 nm.[17,20,21] For designed submicron-sized large NTs, the light scattering can be even more prominent.[22, 23] However, as anodic NTs were grown on Ti metal substrate, the NT layer has to be detached from the substrate to synthesize the free-standing NT film, and then transferred and adhered onto the top of an NP film to act as a light scattering layer.[24–27] Additionally, the NT array suffers from a high concentration of defects, which is likely to induce many trap centers inside the NTs and would cause the poor charge collection and inferior DSSC performance.[28, 29] To

reduce the trap density, the enhancement of NT crystallinity by thermal treatment at a high temperature has been proposed, but the effectiveness is guaranteed only for free-standing NT films.[30]

Inspired by the various hybrid photoanodes consisting of 1D TiO_2 nanostructures,[31, 32] we present a new and straightforward strategy to synthesize TiO_2 NTs in the powder form, and then use them as light scattering centers to improve the solar cell performances. Without the influence of the underlying Ti substrate, highly crystallized NT powders can be obtained by a high-temperature thermal treatment. The efficiencies of the solar cells based on pure NT powders annealed at different temperatures were compared. Furthermore, the NT powders with optimized crystallinity were integrated to the conventional NP photoanode to act as the light scattering assembly. The dependence of the solar cell performance on the NT/NP ratio in the photoanode was investigated in order to achieve the best solar energy conversion efficiency.

Experimental

Preparation of NT powders and NT-NP hybrid paste. A two-step electrochemical anodization was used to grow NT arrays on a pure titanium foil substrate (99.7% purity, Alfa Aesar) with a thickness of 0.89 mm.[33, 34] The anodization was carried out at a constant voltage of 60 V in a fluoride-containing ethylene glycol (EG) electrolyte with 0.5 wt% NH_4F and 3 vol% deionized (DI) water. The as-formed samples were ultrasonicated for 10 min in ethanol to strip off the NT oxide layer from the underlying Ti substrate. The anodization and ultrasonication processes were repeated until the foil was completely consumed. Then the NTs were collected by centrifugation, washed with DI water and ethanol for three times and then dried in vacuum at 120°C overnight to obtain the NT powders. Finally the powders were thermally treated at 550°C, 650°C and 750°C in air with heating and cooling rates of 2°C/min for 2 h to induce crystallization, transforming NTs into the pure anatase phase.

Two types of TiO_2 pastes were synthesized here. Type I pastes were composed of pure NT powders annealed at 550°C, 650°C and 750°C, respectively. The powders were added (10 wt%) to a 1:4 (*v*/*v*) mixture of isopropanol: n-butyl alcohol to prepare the pastes (designated as 550-NT, 650-NT and 750-NT). Type II pastes were composed of both NTs and NPs (the hybrid pastes), prepared by adding the above 650-NT paste to an NP paste (20 nm anatase, Dyesol 18NR-T). The NT/NP ratio in the paste was controlled by adding different weight percentages of 650-NT paste. The mixtures containing 1, 10, 20, 50 and 75 wt% NTs were designated as 1%-NT, 10%-NT, 20%-NT, 50%-NT and 75%-NT, respectively. Here 650-NT sample with pure NTs was also designated as 100%-NT for the convenient comparison. The resultant pastes were well mixed under vigorous stirring at 200 rpm for 24 h before usage. For comparison, the NP paste containing only NPs was also used to fabricate the reference photoanode (designated as 0%-NT).

Fabrication of photoanodes and solar cell assembly. The above mentioned two kinds of TiO_2 pastes were coated on fluorine-doped tin oxide (FTO) conducting glasses (TEC-15, NSG) using a doctor-blade method. The resultant TiO_2 films were dried in air and then sintered at 450°C for 2 h to form good mechanical contacts between the films and the substrates. The eventual thickness was about 8 μm for all the TiO_2 layers. After cooling down to approximately 80°C, the TiO_2 photoanodes were immersed in a N719 dye solution (0.3 mM N719 in 1:1 acetonitrile and tert-butanol by volume, Solaronix) for sensitization at room temperature for 24 h.

For DSSC assembly, the sensitized TiO_2 electrode was rinsed with acetonitrile and dried in air. Then the electrode was covered with a Pt coated FTO glass as the counter electrode, and sealed with a 25 μm thick hot-melt film (SX1170-25, Solaronix) by heating at 120°C. The Pt coated FTO glass counter electrode was fabricated by spin coating H_2PtCl_6 (10 mM in 2-propanol, Advanced) and then thermal decomposition at 420°C for 30 min. The interspace between the two electrodes was infiltrated with a liquid redox electrolyte containing 1.0 M 1,2-dimethyl-3-propyl imidazolium iodide, 0.12 M diiodine, 0.1 M lithium iodide and 0.5 M 4-tertbutylpyridine in 3-methoxypropionitrile by capillarity force.

Structure and photovoltaic performance characterization. The morphologies of various TiO_2 nanostructured photoanodes were analyzed by a field-emission scanning electron microscope (FE-SEM, FEI Sirion 200). Transmission electron microscope (TEM, JEOL JEM-2100F) was used to analyze the microstructure of the NTs. X-ray diffraction (XRD, Cu K_α radiation, Rigaku 9KW SmartLab) was performed to verify the crystal structures. The Brunauer-Emmett-Teller (BET) surface areas were compared by the nitrogen adsorption-desorption isotherms (ASAP 2010, Micromeritics). Samples for measurement were pre-treated at 200°C for 4 h under high vacuum. The surface areas of the different photoanodes were also characterized by the dye-desorption measurements. The dye molecules attached on the TiO_2 film surface were desorbed by putting into a 0.1 M NaOH aqueous solution for 5 min. The absorbance of the dye solution was measured by a UV-vis/NIR spectrophotometer (UV-3600, Shimadzu) to evaluate the dye loading capacity. The transmittance and the diffuse reflectance spectra of the different photoanodes were also obtained by the UV-vis/NIR spectrophotometer.

The corresponding power conversion efficiencies (PCEs) of the assembled DSSCs were determined by a sourcemeter (Model 2420, Keithley) under full sunlight (AM 1.5G, 100 mW cm^{-2}) with an irradiated active area of 0.16 cm^2. A class A solar simulator (450 W, Model 94023A, Newport-Oriel Instruments) was used with an AM 1.5 filter and the light intensity was calibrated using a silicon reference cell (Mono-Si with KG filter, NIST). The incident photon-to-current conversion efficiency (IPCE) spectra in the spectrum range of 400–800 nm were measured by an IPCE measurement kit (Newport-Oriel Instruments) at a short-circuit condition. Electrochemical impedance spectra (EIS) in the frequency range of 0.1 Hz to 100 MHz were carried out in the dark with an electrochemical

workstation (CHI 660C, CH Instruments). The applied bias voltage was the same as the open-circuit voltage of the solar cells, which was modulated by a small amplitude voltage of 10 mV. The parameters of capacitance and resistance were determined by fitting the impedance spectra to a simple equivalent circuit.

Results and Discussion

To take the advantage of the scattering effect of the NTs and facilitate the NT incorporation, herein the fabrication of NT powders, pure NT photoanodes and NT-NP hybrid photoanodes was proposed. The schematic of the fabrication process is shown in Fig. 1. First, aligned NT arrays were grown on a Ti foil substrate by electrochemical anodization. The NTs were densely packed with a film thickness of about 20 μm, which is shown in Fig. S1. Then the as-formed NTs were ultrasonically dispersed in ethanol and collected to synthesize the NT powders. Afterwards the powders were thermally treated at various temperatures to induce crystallization. Finally the crystallized powders were made into the NT pastes, followed by coating directly onto FTO glass substrates to form the type I electrodes. Alternatively, by adding the NT paste to the conventional NP paste, a hybrid NT-NP paste can be obtained. We then deposited the paste onto FTO glass substrates to form the type II hybrid electrodes.

In type II electrode configuration, the embedded NTs can serve as the light scattering centers. When the incident light reaches the hybrid photoanode, the light would be scattered and trapped inside the TiO_2 layer, extending the effective light path in the solar cells. As a result, the recycling of light inside the photoanode strengthens the capture and utilization of photon energy. Compared with the typical double-layered photoanode with scattering capacity constructed by the deposition of a separate scattering layer on the top of a TiO_2 NP film,[4, 9, 35] the incorporation of the NT scattering centers inside the NP films has many advantages, including the simple synthesis procedures and the excellent physical/electrical contacts between NT and NP components.

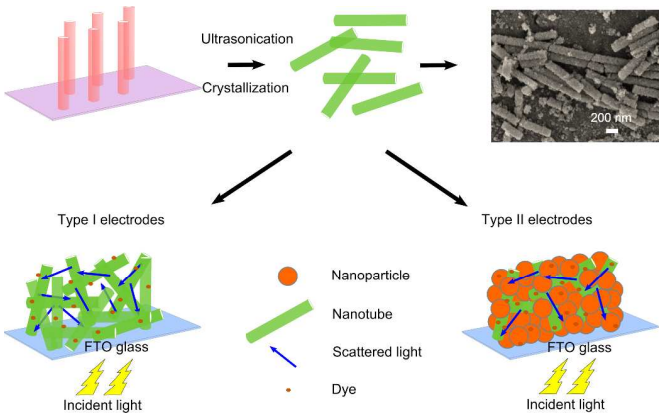

Fig. 1 Schematic representation of the fabrication process of the NT powders and two different types of photoanodes (type I: pure NTs; type II: NT-NP composites). The insert shows the corresponding SEM image of the randomly accumulated NTs in the powder form.

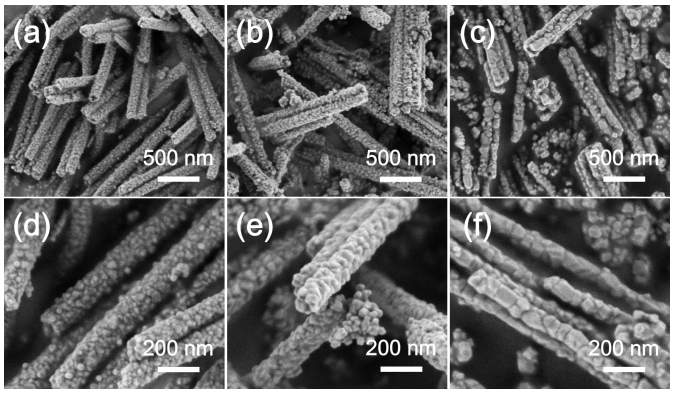

Fig. 2 SEM images of the NT powder samples annealed at (a, d) 550°C, (b, e) 650°C, and (c, f) 750°C, showing the morphological evolution.

The nanostructured morphology of the NT powder is shown in the insert of Fig. 1. As seen from the SEM image, the as-formed closely-packed NT arrays were well dispersed into randomly fragmented NTs, which had lengths in the range of sub to several micrometers. The morphological variation of the NT powders with increasing annealing temperature was shown in Fig. 2. The tubular architecture was maintained at all the temperatures. However, slight change in structural integrity was observed for the samples treated at 750°C, with the appearance of some broken or consolidated tubes. The 1D structure of the NTs was further demonstrated by the TEM images (Fig. 3). After high-temperature crystallization, we can clearly observe large and elongated nano-crystallites existing in the tube walls. For 750°C annealed NTs, the tubes were partially fragmented (Fig. 3c). Compared with the TiO_2 NT bundles fabricated by the detachment, annealing, and grinding of the NT array films[36] or by the rapid breakdown anodization method,[37, 38] the NT powders obtained here were of high quality. According to the XRD patterns (Fig. 4), the diffraction peaks of all the NT samples after annealing at 550°C, 650°C and 750°C can be indexed to the anatase phase. Particularly, the anatase (101)

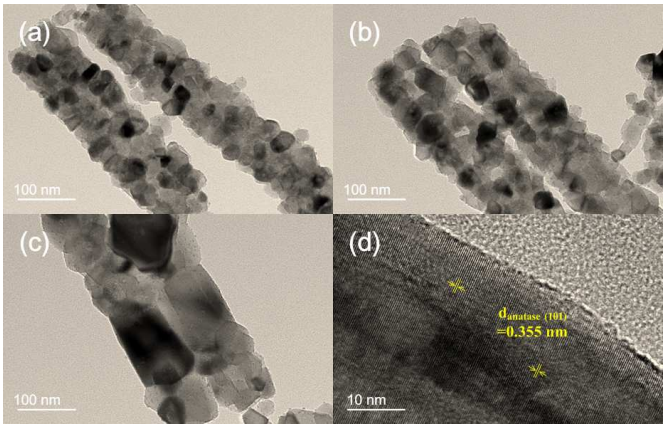

Fig. 3 TEM images of NTs annealed at (a) 550°C, (b) 650°C, and (c) 750°C. (d) The corresponding HRTEM image showing the crystallites in NT walls.

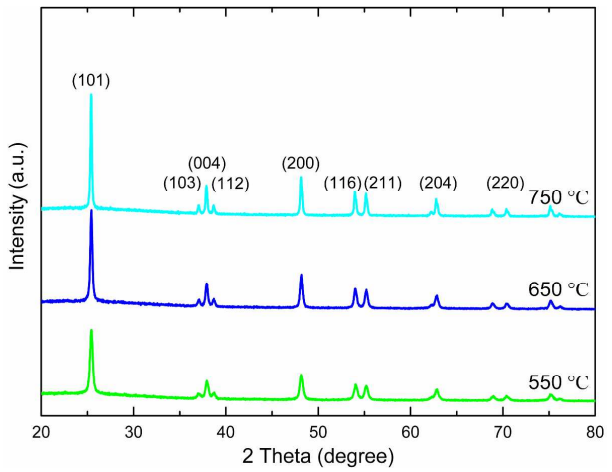

Fig. 4 The XRD patterns of NT powders annealed at different temperatures.

peak intensity increased gradually, indicating an improved degree of crystallization. The HRTEM image shown in Fig. 3d also gives a closer inspection of the nano-crystallites with apparent anatase (101) lattice fringes. The results indicate that after the high-temperature annealing, the crystallinity of the NTs could be greatly enhanced, which is believed to be helpful for the improvement of the charge collection and solar cell performance.

By utilizing the NTs in the powder form, we can easily control the NT/NP ratio of the hybrid paste by incorporating different amounts of NTs into the NP pastes. Visually, the photoanode consisted with typical NP film without any scattering component showed a high transparency in the visible range (0%-NT, Fig. 5a). The NPs have negligible light scattering effect because the size of NPs is much smaller than the wavelength of the visible light. In contrast, with increasing percentage of NTs introduced into the NPs, the film transparency gradually decreased and the photoanode became semi-transparent (1%-NT, 10%-NT, and 20%-NT). After the

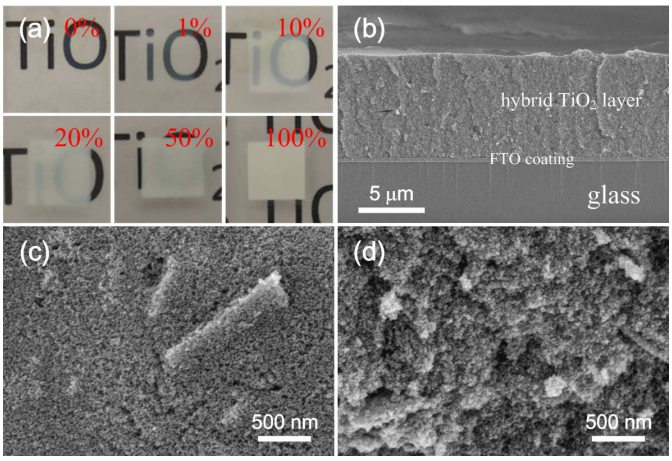

Fig. 5 (a) The photographs of the photoanodes with different NT/NP ratios, showing various film transparencies. (b) The cross-sectional SEM image of the hybrid NT-NP photoanode. The high magnification (c) top-view and (d) side-view SEM images showing the embedment of NTs in the NP network.

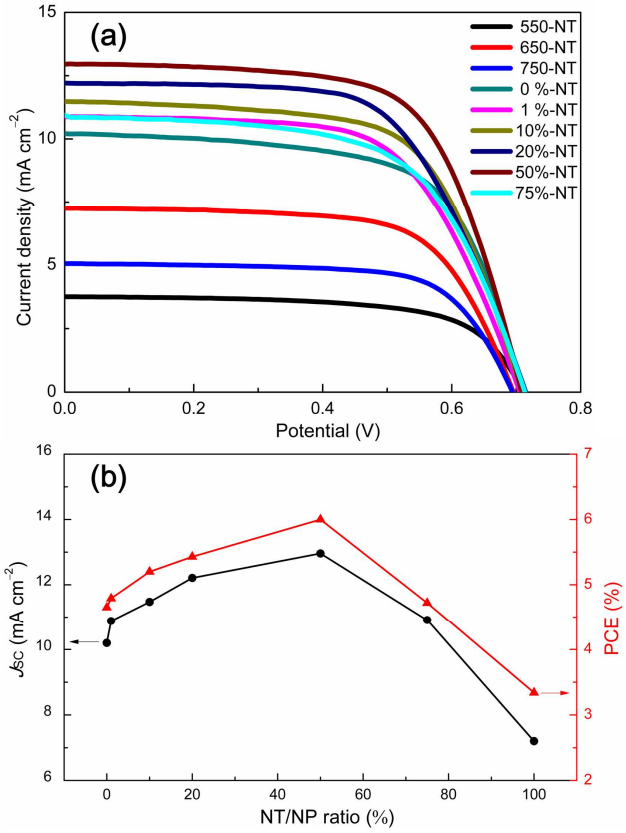

Fig. 6 (a) The photocurrent density-photovoltage characteristics of the DSSCs based on type I and type II electrodes. (b) The dependence of the short-circuit current density and solar cell efficiency on the NT/NP ratio in the electrode.

coupling of high concentration NTs (50%-NT and 100%-NT), the NT-NP hybrid photoanode converted to a non-transparent one. The results demonstrate that NTs had a good scattering ability over the visible region, and by changing the NT/NP ratio, the scattering efficiency was greatly affected.

From the cross-sectional SEM image shown in Fig. 5b, the hybrid NT-NP film fabricated by this strategy was homogeneous, compact and crack-free. The film with a uniform thickness was well connected to the conducting FTO glass substrate. The top-view SEM image also indicates that the hybrid film had a flat and regular top surface (Fig. 5c). After the NT embedment, the NTs were randomly distributed in the NP network. Fig. 5d shows the side-view SEM image of the hybrid film. As the spaces among the NTs could be infiltrated with NPs, little voids were found inside the photoanode. The TEM image of the NT-NP hybrid paste is also shown in Fig. S2. However, in the pure NT based photoanodes (Fig. S3), large-sized NT aggregates were loosely stacked, creating many large voids inside the photoanodes. This would hinder the electron transfer between the neighboring NTs and decrease the specific surface area.

To evaluate the scattering effect of NTs on the enhancement of solar cell efficiency, the photocurrent density-photovoltage (IV) characteristics of pure NT films (type I) and NT-NP hybrid

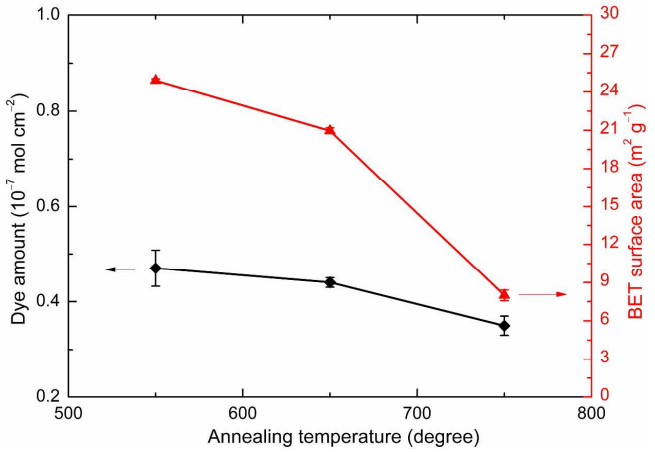

Fig. 7 The dye-loading amounts of type I NT photoanodes and the BET surface areas of NT powders annealed at different temperatures.

films with different NT/NP ratios (type II) were investigated (Fig. 6a). Firstly, the dependence of the type I solar cell efficiencies on the heat treatment temperatures was discussed. By increasing the temperature, both the photocurrent density and the efficiency were improved. The DSSCs based on the 650°C-annealed NTs (650-NT) showed the optimized power conversion efficiency (PCE) of 3.34%. Without the influence of Ti metal substrate, improved NT crystallinity can be obtained by a high-temperature heat treatment. The highly crystallized NTs have been found to be useful to the enhancement of charge collection and solar cell efficiency.[30, 39] However, for the pure NT samples, the optimized cell efficiency (3.34%) remained much lower than that of the reference NP solar cell (0%-NT) with a similar thickness, which showed a PCE of 4.65%. As has been discussed above, in the pure NT electrodes (type I), the NT aggregates were loosely connected, resulting in small internal surface areas, low dye adsorption, and slow electron diffusion through the films, deteriorating the solar cell performances.

Given that the NT powders annealed at 650°C had the optimized crystallinity, we then mixed them with NPs at different ratios to fabricate the NT-NP hybrid photoanodes. The photovoltaic performances of the DSSCs based on these photoanodes are also shown in Fig. 6a. The photocurrent densities gradually increased with increasing NT/NP ratios up to 50%, leading to the improved PCEs. The NT-NP hybrid solar cell with 50 wt% NTs (50%-NT) showed the highest short-circuit current density (J_{SC}) of 12.96 mA cm^{-2}, the open-circuit voltage (V_{OC}) of 0.71 V, the fill factor (*FF*) of 65.3%, and the highest PCE of 6.00%. For comparison, the pure NP cell (0%-NT) with a similar thickness showed the J_{SC} of 10.20 mA cm^{-2}, the V_{OC} of 0.71 V, the *FF* of 64.2%, and the PCE of 4.65%. The NT-NP hybrid solar cell provided a maximum PCE increase of approximately 29% as compared with the solar cell based on pure NPs. The V_{OC} showed little change for all the samples, in the range of 0.69–0.71 V. However, for higher NT/NP ratios (75%-NT and 100%-NT), the efficiency sharply decreased, primarily because of the poor structure of the electrodes mainly composed with NTs. Unlike the results reported previously with the optimized 5–10% NT concentration,[11,12] increasing the NT ratio here played a positive role in boosting the efficiency. This may be attributed to the highly-crystallized and high-quality NTs with multi-functions for the enhancement of the solar cell performances. The variations of J_{SC} and PCE as a function of NT/NP ratio are shown in Fig. 6b and the detailed photovoltaic parameters were summarized in Table 1.

We further compared the dye amounts adsorbed on these photoanodes with different configurations by dye-desorption experiment. The dye-loading amounts per unit electrode area of 550-NT and 650-NT samples were similar, while that of 750-NT decreased significantly, as indicated in Fig. 7. Because the tubes in the pure NT photoanodes were loosely packed, many large pores or voids would exist inside the film, and thus the dye-loading amounts were all very low. Furthermore, the BET specific surface areas of the NT powders annealed at 550°C, 650°C, and 750°C were determined by the nitrogen-sorption analysis, which were 24.9, 21.0, and 8.0 m²/g, respectively (shown in Fig. 7). The variation trend of the surface areas was consistent with that of the dye-loading amounts, with a sharp surface area decrease for the 750°C sample. Although the morphology and phase of the NTs remained stable after 750°C annealing, the tubes were more or less fused together (inner small pores disappeared), leading to much less internal surface area accessible for dye molecules.

Table 1 The photovoltaic parameters and the adsorbed dye amounts of DSSCs based on pure NTs annealed at 550–750°C and NT-NP hybrid films with NT/NP ratios in the range of 0–75%.

Devices	J_{SC} (mA cm^{-2})	V_{OC} (V)	*FF* (%)	PCE (%)	Dye amount ×10^{-7} (mol cm^{-2})
550-NT	3.76	0.71	65.3	1.75	0.47
650-NT (100%-NT)	7.20	0.70	66.8	3.34	0.44
750-NT	5.06	0.69	69.1	2.42	0.35
0%-NT	10.20	0.71	64.2	4.65	1.00
1%-NT	10.88	0.71	62.4	4.79	0.98
10%-NT	11.47	0.71	64.1	5.20	0.93
20%-NT	12.21	0.71	62.2	5.43	0.89
50%-NT	12.96	0.71	65.3	6.00	0.80
75%-NT	10.91	0.71	60.8	4.72	0.63

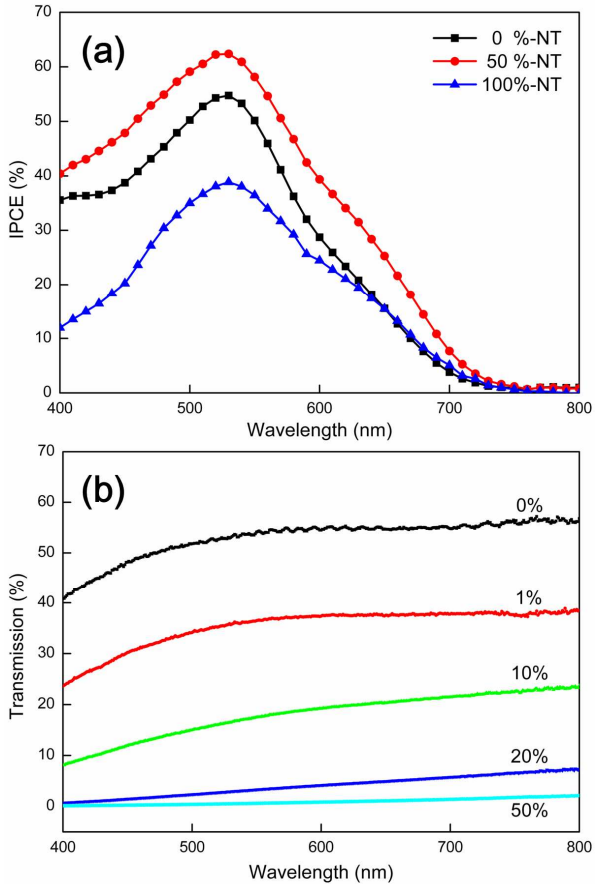

Fig. 8 (a) The IPCE spectra of the hybrid NT-NP structures with the NT/NP ratios of 0, 50 and 100%. (b) The transmission spectra of the samples with 0, 1, 10, 20, and 50% NT concentrations, respectively.

Among different photoanodes, the dye-loading amount of the conventional NP photoanode was the largest. Since the surface area of pure NTs was smaller than that of NPs,[40] the incorporation of the NTs would affect the dye-loading capacity of the hybrid photoanodes. The amounts of the adsorbed dyes of the hybrid photoanodes slowly decreased with increasing NT content. Compared with the NP photoanode, the less dye loading of a hybrid photoanode caused the decreased light harvesting, but this drawback could be overcome by the significant light scattering of the NTs in the solar cells, leading to eventually enhanced light harvesting, and thus improved photocurrent densities and solar cell efficiencies.

The external quantum efficiencies from the IPCE spectra confirmed the enhancement of the photocurrent densities of the NT-NP hybrid photoanodes. As can be seen in Fig. 8a, the 50%-NT sample exhibited a much higher quantum efficiency

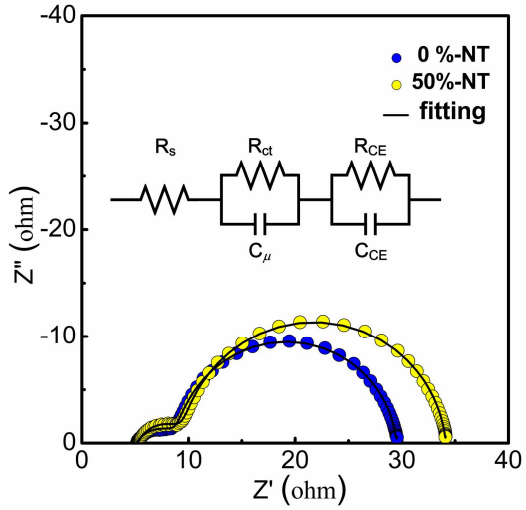

Fig. 9 EIS Nyquist plots under the open-circuit condition of the 0%-NT and 50%-NT samples. The plots were fitted with an equivalent circuit shown in the insert.

than the pure NP (0%-NT) solar cell over the entire wavelength region (400–800 nm). In detail, the peak efficiency increased from 55% for 0%-NT sample to 62% for 50%-NT sample at a wavelength of 530 nm. A recent analysis has demonstrated the superior electron diffusion length in the highly-crystallized NTs than in the conventional NTs and NPs.[30] The efficient electron collection through the highly-crystallized NT incorporated photoanode was responsible for the enhanced efficiency. It is also noted that the efficiency gap between 0%-NT and 50%-NT samples was greater in the long wavelength region from 600–800 nm. This was attributed to the superior light scattering capability of the NTs embedded in the NP films, especially at the long wavelengths. In particular, it is clearly shown in Fig. 8a that for the pure NT photoanodes, although the peak efficiency was much lower, the efficiency at the long wavelengths was comparable to that of the pure NPs. This suggests that the strong scattering effect of the NTs can promote the long-wavelength light absorption inside the photoanodes and thus enhance the photocurrent densities of the solar cells.

As has been discussed above, when the NTs were integrated into the NP films, the film transparency significantly decreased with increasing NT contents. This can also be observed from the light transmission spectra of these films in Fig. 8b. For example, introducing 1% NTs into the NP film would lead to a 33% decrease in the film transparency at 530 nm. When the NT/NP ratio in the hybrid film exceeded 50%, the film exhibited a very low transmittance and almost no light could

Table 2 The interfacial resistances and capacitances of DSSCs based on the 0%-NT and 50%-NT photoanodes.

Devices	R_s (Ω)	R_{ct} (Ω)	C_μ (mF cm^{-2})	R_{CE} (Ω)	C_{CE} (mF cm^{-2})
0%-NT	5.12	19.55	2.36	4.02	0.76
50%-NT	5.25	24.02	1.91	4.39	0.40

R_s, series resistance; R_{ct}/C_μ and R_{CE}/C_{CE}, resistance/capacitance at the TiO_2/electrolyte and counter electrode/electrolyte interfaces; τ_n, electron lifetime.

transmit through the photoanode. The diffuse reflectance spectra of the photoanodes with 0–100% NTs provide further evidence of the strong scattering effect of the NTs (Fig. S4). With increasing NT ratios in the hybrid films, the light reflectance increased gradually over the whole visible range of 400–800 nm. Particularly, the peak reflectance of the 50%-NT sample was around 66%, much higher than that of the NP electrode (22%). As a result, the NTs embedded in the NPs are suitable for the light harvesting improvement in DSSCs.

Furthermore, the electrochemical behaviors of the NT-NP hybrid solar cells was analyzed by the EIS measurement.[41] Fig. 9 shows the Nyquist plots of EIS which were fitted using an equivalent circuit R_s-R_{ct}/C_μ-R_{CE}/C_{CE} shown in the insert. It can be directly observed that the radius of the semicircle at intermediate frequencies (the main arc) of 50%-NT sample was larger than that of 0%-NT sample. This indicates an increase in the electron transfer resistance (R_{ct}) and a reduction in the electron recombination rate with the oxidized species at the TiO_2/electrolyte interfaces for the NT-NP cell with respect to the NP cell. According to the fitting results listed in Table 2, the R_{ct} of the NT-NP solar cell showed a higher value (24.02 Ω) than that of NP one (19.55 Ω). It is also found that the chemical capacitance (C_μ) of the NT-NP electrode (1.91 mF cm^{-2}) was lower than that of the NP one (2.36 mF cm^{-2}), which implies the lower defect centers and/or trap density for the highly crystallized 650-NT sample.[42] The apparent electron lifetime (τ_n) can thus be estimated by the equation $\tau_n=R_{ct}\times C_\mu$. The result shows that τ_n in the 650-NT solar cell was similar to that in the NP solar cell (45.9 ms for NT-NP cell vs. 46.1 ms for NP cell), which is consistent with the observed similar V_{OC} of the solar cells.

Conclusions

In summary, we developed a new kind of nanostructured photoanodes containing TiO_2 NPs and NTs for efficient light harvesting in high-performance DSSCs. The NT powders can be readily fabricated by electrochemical anodization and ultrasonic dispersion. Then the NT powders were made into paste, and then coated on the FTO glass substrates to fabricate the pure NT photoanodes. The crystallinity of the NT powders was optimized to reach the highest DSSC efficiency. Furthermore, the NT paste was mixed with the NP paste to synthesize the NT-NP hybrid paste, and corresponding NT-NP hybrid photoanodes. This hybrid configuration was proposed to possess pronounced light scattering effect, high dye-loading capacity, as well as efficient electron collection. Suitable adjustment of the NT/NP ratios in the photoanodes can maximize the light harvesting of the DSSCs. Despite the 33% lower dye-loading amount, the PCEs of the solar cells based on the hybrid photoanodes could be improved up to 29% compared with the conventional NP devices.

Acknowledgements

The work was supported by the National Natural Science Foundation of China (Grant Nos. 61125503, 61404081, 11374204, and 11204172), the Shanghai Municipal Natural Science Foundation (Grant No. 14ZR1417700), and the "Chen Guang" project supported by Shanghai Municipal Education Commission and Shanghai Education Development Foundation.

Notes and references

[a] Department of Physics, Shanghai University of Electric Power, 2103 Pingliang Road, Shanghai 200090, China;
[b] Department of Physics and Astronomy, Shanghai Jiao Tong University, 800 Dongchuan Road, Shanghai 200240, China.
E-mail: xfchen@sjtu.edu.cn

1 B. O'regan and M. Grätzel, *Nature*, 1991, **353**, 737.
2 B. E. Hardin, H. J. Snaith and M. D. McGehee, *Nat. Photonics*, 2012, **6**, 162.
3 H. J. Snaith and L. Schmidt-Mende, *Adv. Mater.*, 2007, **19**, 3187.
4 S. Ito, T. N. Murakami, P. Comte, P. Liska, C. Grätzel, M. K. Nazeeruddin and M. Grätzel, *Thin Solid Films*, 2008, **516**, 4613.
5 S. Hore, C. Vetter, R. Kern, H. Smit and A. Hinsch, *Sol. Energy Mater. Sol. Cells*, 2006, **90**, 1176.
6 I. G. Yu, Y. J. Kim, H. J. Kim, C. Lee and W. I. Lee, *J. Mater. Chem.*, 2011, **21**, 532.
7 S. Dadgostar, F. Tajabadi and N. Taghavinia, *ACS Appl. Mater. Interfaces*, 2012, **4**, 2964.
8 J. Feng, Y. Hong, J. Zhang, P. Wang, Z. Hu, Q. Wang, L. Han and Y. Zhu, *J. Mater. Chem. A*, 2014, **2**, 1502.
9 H.-Y. Chen, T.-L. Zhang, J. Fan, D.-B. Kuang and C.-Y. Su, *ACS Appl. Mater. Interfaces*, 2013, **5**, 9205.
10 S. H. Hwang, C. Kim, H. Song, S. Son and J. Jang, *ACS Appl. Mater. Interfaces*, 2012, **4**, 5287.
11 J. Sheng, L. H. Hu, S. Y. Xu, W. Q. Liu, L. e. Mo, H. J. Tian and S. Y. Dai, *J. Mater. Chem.*, 2011, **21**, 5457.
12 A. Lamberti, A. Sacco, S. Bianco, M. Quaglio, D. Manfredi and C. F. Pirri, *Microelectron. Eng.*, 2013, **111**, 137.
13 D. A. Wang, B. Yu, F. Zhou, C. W. Wang and W. M. Liu, *Mater. Chem. Phys.*, 2009, **113**, 602.
14 X. Zhang, H. Liu, X. Huang and H. Jiang, *J. Mater. Chem. C*, 2015, **3**, 3336.
15 S. Wooh, H. Yoon, J. H. Jung, Y. G. Lee, J. H. Koh, B. Lee, Y. S. Kang and K. Char, *Adv. Mater.*, 2013, **25**, 3111.
16 Y.-J. Chang, E.-H. Kong, Y.-C. Park and H. M. Jang, *J. Mater. Chem. A*, 2013, **1**, 9707.
17 K. Zhu, N. R. Neale, A. Miedaner and A. J. Frank, *Nano Lett.*, 2007, **7**, 69.
18 D. B. Kuang, J. Brillet, P. Chen, M. Takata, S. Uchida, H. Miura, K. Sumioka, S. M. Zakeeruddin and M. Grätzel, *ACS Nano*, 2008, **2**, 1113.
19 C.-T. Yip, H. T. Huang, L. M. Zhou, K. Y. Xie, Y. Wang, T. H. Feng, J. Li and W. Y. Tam, *Adv. Mater.*, 2011, **23**, 5624.

20 L. L. Li, C. Y. Tsai, H. P. Wu, C. C. Chen and E. W. G. Diau, *J. Mater. Chem.*, 2010, **20**, 2753.
21 H. G. Yun, J. H. Park, B. S. Bae and M. G. Kang, *J. Mater. Chem.*, 2011, **21**, 3558.
22 X. Liu, M. Guo, J. Lin, X. Chen and H. Huang, *RSC Adv.*, 2014, **4**, 45180.
23 Y. Zhang, J. Khamwannah, H. Kim, S. Y. Noh, H. Yang and S. Jin, *Nanotechnology*, 2013, **24**, 045401.
24 Q. Zheng, H. Kang, J. Yun, J. Lee, J. H. Park and S. Baik, *ACS Nano*, 2011, **5**, 5088.
25 J. Luo, L. Gao, J. Sun and Y. Liu, *RSC Adv.*, 2012, **2**, 1884.
26 X. Liu, M. Guo, J. Cao, J. Lin, Y. H. Tsang, X. Chen and H. Huang, *Nanoscale Res. lett.*, 2014, **9**, 362.
27 X. K. Xin, J. Wang, W. Han, M. D. Ye and Z. Q. Lin, *Nanoscale*, 2012, **4**, 964.
28 Y. Yu, K. J. Wu and D. L. Wang, *Appl. Phys. Lett.*, 2011, **99**, 192104.
29 P. Docampo, S. Guldin, U. Steiner and H. J. Snaith, *J. Phys. Chem. Lett.*, 2013, **4**, 698.
30 J. Lin, M. Guo, C. T. Yip, W. Lu, G. Zhang, X. Liu, L. Zhou, X. Chen and H. Huang, *Adv. Funct. Mater.*, 2013, **23**, 5952.
31 B. Tan and Y. Wu, *J. Phys. Chem. B*, 2006, **110**, 15932.
32 P. Joshi, L. Zhang, D. Davoux, Z. Zhu, D. Galipeau, H. Fong and Q. Qiao, *Energy Environ. Sci.*, 2010, **3**, 1507.
33 J. Lin, J. F. Chen and X. F. Chen, *Electrochem. Commun.*, 2010, **12**, 1062.
34 G. Zhang, H. Huang, Y. Zhang, H. Chan and L. Zhou, *Electrochem. Commun.*, 2007, **9**, 2854.
35 T. Deepak, G. Anjusree, S. Thomas, T. Arun, S. V. Nair and A. S. Nair, *RSC Adv.*, 2014, **4**, 17615.
36 C.-J. Lin, W.-Y. Yu and S.-H. Chien, *Appl. Phys. Lett.*, 2007, **91**, 233120.
37 N. F. Fahim and T. Sekino, *Chem. Mater.*, 2009, **21**, 1967.
38 K. S. Lee, J. Kwon, J. H. Im, C. R. Lee, N.-G. Park and J. H. Park, *ACS Appl. Mater. Interfaces*, 2012, **4**, 4164.
39 T. Zeng, H. Ni, X. Su, Y. Chen and Y. Jiang, *J. Power Sources*, 2015, **283**, 443.
40 A. Kongkanand, K. Tvrdy, K. Takechi, M. Kuno and P. V. Kamat, *J. Am. Chem. Soc.*, 2008, **130**, 4007.
41 R. Kern, R. Sastrawan, J. Ferber, R. Stangl and J. Luther, *Electrochim. Acta*, 2002, **47**, 4213.
42 C. Di Valentin, G. Pacchioni and A. Selloni, *J. Phys. Chem. C*, 2009, **113**, 20543.

Graphical Abstract

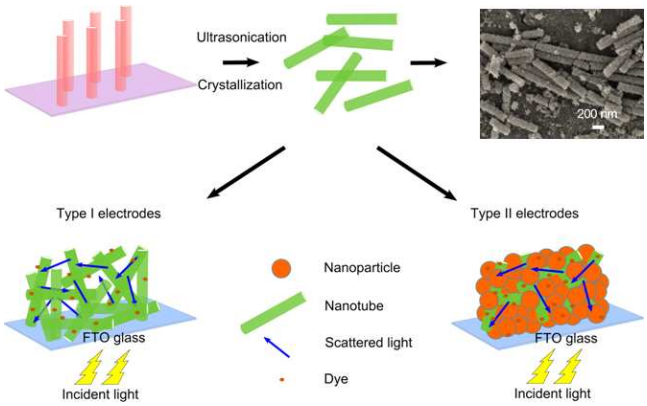

Highly crystallized TiO_2 nanotube (NT) powders were fabricated and incorporated into TiO_2 nanoparticle (NP) films to form NT-NP hybrid photoanodes.